Title

Evaluation of Condylar Adaptation after Unilateral Loss of Maxillary Molar Extractions in Skeletally and Dentally Mature Mice

Permalink

https://escholarship.org/uc/item/8gr1t7f0

Author

Huang, Jessica L

Publication Date

2024

Peer reviewed|Thesis/dissertation

Evaluation of Condylar Adaptation after Unilateral Loss of Maxillary Molar Extractions in Skeletally and Dentally Mature Mice

by
Jessica L Huang

THESIS
Submitted in partial satisfaction of the requirements for degree of
MASTER OF SCIENCE

in

Oral and Craniofacial Sciences

in the

GRADUATE DIVISION
of the
UNIVERSITY OF CALIFORNIA, SAN FRANCISCO

Approved:

DocuSigned by:

Christine Hong
CE6EAA6FBA31451...
_____
Christine Hong
Chair

DocuSigned by:

Mona Bajestan
DocuSigned by: ...4B2...
_____
Mona Bajestan

Alice Goodwin
C8CADA453C824D9...
_____
Alice Goodwin

_____

_____
Committee Members

ACKNOWLEDGEMENTS

Evaluation of Condylar Adaptation after Unilateral Maxillary Molar Extraction

in Skeletally and Dentally Mature Mice

Jessica L Huang

ABSTRACT

The temporomandibular joint (TMJ) is a complex structure that joins the temporal bone to the mandible in order to facilitate mastication and speech. All the components of the TMJ must work in tandem with the contralateral side to produce the dynamic movements required for speech and mastication. Any dysfunction between the two TMJs or within one TMJ itself may lead to painful or non-painful temporomandibular disorders (TMDs). There is a wide range of causes for TMDs, including biomechanical, biological, and bio-psychosocial factors, but there are limited treatment options available due to a lack of understanding of the etiology and pathogenesis of TMDs. In order to provide improved interventions and treatment, there needs to be a better understanding of the etiopathogenesis of TMDs at the tissue, cellular, and molecular level. One specific area of interest is the mandibular condylar cartilage (MCC), which has been shown to undergo cellular changes in response to altered occlusion in mice. The aim of this study was to examine how the TMJ responds to altered occlusion (unilateral maxillary molar tooth extractions) in skeletally and dentally mature mice to better understand the adaptive potential of the TMJ and progression of occlusal-related TMDs. The results showed that there were no changes in morphology of the condyle or cellular organization of the MCC in adult mice after extraction of the 3 maxillary right molars, and thus, no adaptive changes occur in response to altered occlusion in skeletally mature mice with stable occlusion.

TABLE OF CONTENTS

LIST OF FIGURES

LIST OF TABLES

LIST OF ABBREVIATIONS

FDR – false discovery rate

GMA – geometric morphometric analysis

HA – hyaluronic acid

MCC – mandibular condylar cartilage

OA – osteoarthritis

PCA – principal component analysis

RA – rheumatoid arthritis

TMD – temporomandibular joint disorders

TMJ – temporomandibular joint

INTRODUCTION

Structure and function of the temporomandibular joint

The temporomandibular joint (TMJ) is a complex structure that is an essential part of the masticatory system and necessary for speech production. In simple terms, the TMJ is the point within the skull where the lower jaw meets the upper jaw. The upper and lower jaws also contact each other by means of teeth, while the surrounding ligaments and muscles help drive the mandible to move. Unlike other joints in the body, the TMJ is paired, so if one side is affected there can be side effects to the contralateral side. In addition, issues that arise within the teeth, ligaments, or muscles of the face can indirectly cause problems to the TMJs.

The TMJ is the only ginglymoarthrodial joint in the body because it performs both rotational (ginglymoid) and translational (arthrodial) movements. It joins the mandibular condyle to the temporal bone at the glenoid fossa, joint capsule, and articular disc. The articular disc sits between the condyle and glenoid fossa. It is a biconcave cartilaginous disc that functions to cushion the mandibular condyle as it rotates and to absorb the forces that are constantly exerted on the bony structures. The TMJ is protected by a fibrous capsule. There are numerous ligaments and muscles that attach the mandible to the skull to facilitate chewing and speech. Ligaments of the TMJ include the temporomandibular (lateral ligament), sphenomandibular, and stylomandibular ligaments, which help provide proprioceptive stimuli for the TMJ. The muscles that elevate the mandible include the masseter, temporal, and inferior head of the lateral pterygoid muscle. The muscles that depress the mandible are the medial pterygoid, geniohyoid, mylohyoid, and digastric muscles. The muscle that is directly attached to the articular disc is the superior head of the lateral pterygoid muscle. All the components of the TMJ must work in tandem with the contralateral TMJ to produce the dynamic movements required for speech and mastication.

1

Mandibular condylar cartilage

The mandibular condylar cartilage (MCC) is different compared to the condylar heads of other joints in that it is composed of secondary cartilage, instead of primary cartilage (Velasco, 2009). Primary cartilage develops in response to systemic growth stimuli, such as hormones, and the cartilage is eventually replaced by bone. Secondary cartilage only develops after primary cartilage and in response to local growth factors (Shen, 2005). Secondary cartilage does not get replaced by bone as it remains cartilage throughout life as it proliferates with an appositional organization. The appositional growth of the MCC contributes to the overall growth of the mandible. The main role of the MCC is to provide a frictionless movement of the condyle within the glenoid fossa and along the articular eminence. Unlike other articular cartilages, the MCC is the only articular cartilage with the ability to remodel and adapt in response to mechanical loading during mastication or changes in condylar positioning with altered occlusion (Shen, 2005).

The MCC is the most superior portion of the condylar head and is composed of 4 zones (Singh, 2009). From a superior to inferior direction, the first layer is the fibrous zone, proliferative zone, mature zone, and lastly the hypertrophic zone. The fibrous zone contains fibrocartilage stem cells, which then undergo a proliferative phase and begin to express several genes, including *Col1a1*, *Sox9*, and *Runx2* within the proliferative zone. These cells further differentiate and grow into mature chondrocytes in the mature zone, and eventually become large hypertrophic chondrocytes within the hypertrophic zone. In order to better understand the cellular changes and gene expression in the MCC in response to altered occlusion, close examination is needed.

Temporomandibular joint disorders

Dysfunction between the two TMJs or within one TMJ itself can lead to temporomandibular disorders (TMDs). TMDs can range from non-painful joint noises to

debilitating signs and symptoms that often result in chronic facial pain and decreased quality of life. The prevalence is still unclear and may be underreported, but a systematic review reported a frequency between 3.4% to 65.7% for painful TMD symptoms and 3.1% to 40.8% for non-painful symptoms (Lai, 2020). The same study also reported 10.6% to 68.1% of males were affected, while 21.2% to 72.4% of females were affected, and noted that TMD prevalence was higher among females in all the studies. The wide range of reporting reflects the complexity in diagnosing TMDs. Additionally, the etiology and pathogenesis of TMDs is multifactorial and can stem from biomechanical, biological, and bio-psychosocial factors (Chisnoiu, 2015). Biomechanical factors include parafunctions, trauma, and occlusal overloading. However, there is conflicting evidence with studies showing both association and no association between TMD and occlusion (Lai, 2020). Biological factors can include increased levels of estrogen or degenerative joint diseases such as OA or osteoarthritis (Tanaka, 2008). Lastly, bio-psychosocial factors can include stress, anxiety, and depression (Chisnoiu, 2015). Management of TMDs is limited with a few non-invasive and minimally invasive procedures with about 5% of patients eventually requiring surgery (Alowaimer, 2024). There may be limited treatment due to a lack of understanding of the etiology and pathogenesis of TMDs. In order to provide improved interventions and treatment, there needs to be a better understanding of the etiopathogenesis of TMDs at the tissue and cellular level.

There is a long-standing controversy regarding the relationship between occlusion and TMDs. Some individuals believe that malocclusion, whether skeletal or dental in the sagittal, transverse, or vertical planes, can be prevented or cured by achieving occlusal harmony with orthodontics (Michelotti, 2020). Conversely, other patients believe that orthodontic therapy, including extractions as part of treatment, was the source of their TMDs. A review of the literature has found that there is no association between orthodontics and TMDs (McNamara, 1995) and that orthodontics can not cure TMDs (Shroff, 2018). There are also patients who perceive their TMDs were triggered by dental treatment (Mitrirattanakul, 2018). The confounding

perceptions and evidence calls for further investigation on the relationship between TMDs and occlusion.

Preliminary studies

Rodent models have been widely used to study mandibular adaptation to altered occlusion, specifically using oral appliances (Jung, 2014). The use of these appliances relies heavily on the operator and are challenging to place, often leading to inconclusive results. An extraction model on rodents is a more reliable alternative, as it does not require the use of any oral appliances and is more economical. Chen et al. (2022) conducted a preliminary study on the adaptive response of the TMJ and MC to the extraction of molars in juvenile mice. They extracted all three molars from the maxillary right quadrant in 3-week-old (pre-pubertal) mice, and then analyzed them three weeks later at 6-weeks of age for any morphological, tissue, cellular, and molecular changes of the MC. The results showed that unilateral loss of the maxillary right molars led to significant bilateral changes in the condylar morphology. Geometric morphometric analysis (GMA) was used to analyze the changes, which included antero-posterior narrowing of the head and neck of the condyle, and increased convexity at the condylar surface. The experimental mice also showed decreased bone volume by ~15%, and increased bone mineral density near the condylar head of ~5%. These alterations in condylar bone occurred in conjunction with cellular changes, which suggests degenerative changes transpired. Histomorphometry was also performed to analyze condylar adaptive changes, and the results showed increased expression of the chondrocyte markers *Col2a1* and *Col10a1*, which suggests increased maturation and hypertrophic chondrocytes in response to altered occlusion. Overall, the changes suggest that the mandibular condyle undergoes tissue, cellular, and molecular changes in response to altered occlusion in pre-pubertal mice. In order to understand the effect of altered occlusion on the TMJ without the effect of growth, a new study needed to be performed on skeletally mature mice with occlusion in homeostasis and with

condyles that were no longer actively growing. The aim of this study was to examine how the TMJ responds to altered occlusion (unilateral maxillary molar tooth extractions) in skeletally and dentally mature mice to better understand the adaptive potential of the TMJ and progression of occlusal-related TMDs.

CENTRAL HYPOTHESIS

Null hypothesis

There are no changes in morphology or cellular composition of the condyle in skeletally mature mice after extraction of the 3 maxillary right molars, and thus, no adaptive changes occur in response to altered occlusion.

Alternative hypothesis

There are changes in morphology and/or cellular composition of the condyle in skeletally mature mice after extraction of the 3 maxillary right molars, thus indicating that adaptive changes occur in response to altered occlusion.

SPECIFIC AIMS

Aim 1

Determine changes in morphology of the mandible and skull 3 weeks after tooth extraction in adult mice using microCT and GMA.

Aim 2

Examine the mandibular condylar cartilage (MCC) at the tissue and cellular level using H&E staining and RNAscope.

MATERIALS AND METHODS

Animals

FVB/NJ mice were obtained from the Jackson Laboratory (Strain #:001800) and bred in the Goodwin Lab mouse colony. All the mice were fed and housed under the same conditions. All animal care, procedures and experiments were approved by the Institutional Animal Care and Use Committee (IACUC) at UCSF (Protocol AN182286). Experimental mice were anesthetized with ketamine and xylazine at 8 weeks of age (P56). The mice were stabilized in a plaster cast with tape, a mouth proper, and cheek retractors, and all 3 molars of the maxillary right quadrant were extracted using fine tipped tweezers (Figure 1B). The control mice also underwent anesthesia and stabilization in the plaster cast, however no teeth were extracted. There were 14 experimental mice (7 females, 7 males), and 14 control mice (7 females, 7 males). All the mice were euthanized with CO_2 asphyxiation and cervical dislocation at 11 weeks of age (P77). Heads were removed and fixed in 4% paraformaldehyde.

For the bulk RNA-Sequencing experiment, control and experimental FVB/NJ mice were anesthetized with ketamine and xylazine at 3 weeks of age (P21). The mice were also stabilized with the plaster cast set-up, and the maxillary third molars were extracted from experimental mice. All mice were euthanized two days later to examine gene expression immediately after extractions. The mandibles were removed, and the mandibular condylar cartilage (MCC) was manually dissected in cold PBS using a dissecting scope. The right and left MCC were stored in RNAlater solution for each animal. There were 4 experimental mice (2 females and 2 males), and 4 control mice (2 females, 2 males).

Micro-computed tomography (microCT)

MicroCT was performed on the entire skull of the experimental and control mice at 11 weeks of age using a MicroCT50 (SCANCO Medical AG, Brüttisellen, Switzerland), 55 kVp,

109 µA, 6 W at 20 µm voxel size, with a 500 ms integration time and a 20.5 mm field of view. Sample numbers were selected based on our power calculation that 12 samples were required to detect a 0.1 mm difference at a power of 90%. The microCT data was imported into Avizo Lite software to manually segment the cranium and mandibles. Isosurfaces were generated for the cranium and left and right mandibles.

Geometric morphometric analysis (GMA)

The isosurfaces generated from Avizo Lite were imported into Stratovan Checkpoint software, and the cranium and mandibles were landmarked. The cranium had 44 landmarks, while the mandibles had 26 landmarks (13 landmarks per side) as was used for the preliminary study by Chen et al. (2022), for a total of 1,960 landmarks on 28 mice (Figure 2A, 2B, and Table 1). Two examiners performed the landmarking, and inter-rater reliability was evaluated using principal component analysis (PCA).

The landmark coordinates were imported into MorphoJ software for 3D shape analysis. A Procrustes superimposition was performed to standardize all the images to control for scaler differences between the images. PCA was performed to analyze whether there were any major differences in shape between the control versus experimental groups. PCA is a method to simplify multiple dimensions and project the most important factors onto a 2D plot, while retaining as much information as possible. PCA was also used to assess for significant shape differences between male and female mice.

MorphoJ software was also utilized to create wireframes to visualize any shape variation or similarities from PC1. Three wireframes were generated: maximum, average, and minimum, which were superimposed onto each other for visual comparison.

Histological analysis

Following micro-CT scanning, heads were demineralized in 0.5M EDTA, paraffin

processed and embedded, and sectioned coronally with a microtome (N=3 experimental and 3 control). Hematoxylin and eosin (H&E) staining was performed on the sections to analyze the TMJ and MCC. The widths of the MCC were measured in ImageJ software. RNAscope was performed on coronal sections with specific mouse probes against *Scara5*, *Iqgap2*, and *Cxcl14*.

RNA-sequencing

The MCC was collected from 3-week old control and extraction mice as described. RNA extraction from the tissue was performed using the RNeasy Mini Kit (Qiagen, 74104). RNA sequencing was done on all the samples to look at gene expression at the RNA level. RNA-sequencing (RNA-seq) was performed on an Illumina HiSeq 4000. Read counts were generated, and only mapped reads uniquely assigned to the mouse genome were used for differential expression testing. The expression matrix was imported into R and normalized for sequencing read depth. Quality control plots were created, differential expression was performed using DESeq2 (Wald test), and significant genes were filtered by a threshold of false discovery rate <0.05, $1.5 < \log_2 FC < -1.0$, and raw counts >100. One-hundred and eighteen genes were found with a false discovery rate <0.05, which was narrowed down to 23 genes with at least 1 N=over 100 counts and $1.5 < \log2FC < -1.0$ (biologically significant expression and fold change). No genes were significantly upregulated in the experimental group; all of the genes were significantly downregulated.

RESULTS

Inter-rater reliability tests

Two examiners performed the landmarking of the left mandible, right mandible, and skull in Stratovan Checkpoint, and an inter-rater reliability test was evaluated using principal component analysis (PCA). The PCA for the left and right mandibles showed that there was a discrepancy between the two examiners, as there were two distinct clusters. There were two landmarks that showed consistent discrepancy between examiners. The first landmark (point 6) is the most anterior/inferior concave point of the coronoid process, and the second landmark (point 9) is the most concave point between the condyle and angular process (Figure 3A, 3B). Even though there were two points of disagreement, the outcome of the analysis was the same because the two landmarks were not at the condyle. Both examiners accepted the null hypothesis after analyzing their individual data. These inter-rater reliability test data emphasize the importance of training the examiners and having clear landmark definitions for GMA studies. If this study is to be replicated, then the landmarking should be compared after a few samples to correct any discrepancies. The inter-rater reliability PCA for the skull showed tight and overlapping clusters, which indicates both examiners had similar landmarks.

Extraction of molars in the maxillary right quadrant of skeletally mature mice did not cause morphological changes of the mandible, condyle, or skull

PCA was performed to compare the experimental and control groups for the left mandible, the right mandible, and the skull. The results show no changes in morphology of the mandible, condyle, or skull, thus our null hypothesis holds true (Figure 4A, 4B). For the left mandible, the PCA shows overlapping ellipses with scattered but overlapping data points (Figure 5A). There was minimal variation between the two groups, with 19.09% of the variance accounted for by PC1, and 16.37% by PC2 (Figure 5C, and Table 2). The wireframes show

11

almost complete overlapping between PC1 minimum and PC1 maximum (Figure 5D). The area

of most discrepancy within the wireframes is seen at the angular process, however, as shown

by the PCA, the shape differences between groups were not significant. There are no noticeable

differences between the isosurface images when comparing the experimental and control

groups. PCA was also performed to compare the experimental and control groups by sex, and

the results show no difference between males and females (Figure 5B).

There were similar results for the right mandible, in which the PCA shows overlapping

groups so there were no morphological changes between the experimental and control groups

(Figure 6A). PC1 only accounted for 18.93% of the variance, while PC2 contributed 15.8% of

the variance (Figure 6C, and Table 3). The wireframe diagrams for PC1 minimum and PC1

maximum of the right mandible are nearly identical (Figure 6D). Once again, there are no

obvious differences between the isosurface images of the two groups (Figure 6B). When

comparing males and females, the PCA showed no difference.

Even though the focus of this study is on the mandibular condyle, we analyzed the skull

to assess whether extraction of all molars in the maxillary right quadrant caused any adaptive

changes to the maxilla. The results show no difference in morphology of the maxilla or skull

between the experimental and control groups. The PCA showed overlapping ellipses with PC1

accounting for 29.77% of the variance, and PC2 accounting for 16.68% of the variance (Figure

7A, 7B, and Table 4). No wireframes were performed for the skull due to the large amount of

landmarks. There was no difference between males and females as seen in the PCA (Figure

7B).

Overall, the results indicate that there are no changes in morphology of the condyle in

skeletally mature mice after extraction of the 3 maxillary right molars, and thus, no adaptive

changes occur in response to altered occlusion in adult mice.

Extraction of molars in the maxillary right quadrant of skeletally mature mice did not cause cellular changes to the mandibular condylar cartilage

In order to investigate if there were any cellular changes in the MCC with maxillary right molar extraction in adult mice, we performed H&E staining and RNAscope. The condyles were sectioned coronally and the widths of the MCC were measured in ImageJ software to see if there were differences between the left and right condyles and between experimental and control mice. There were 3 experimental and 3 control mice, however, one of the experimental samples could not be measured because there was a lack of adequate sections due to sectioning errors. Since we were unable to examine 3 experimental samples, there were not enough samples to perform a statistical analysis. The width of the MCC was measured in microns at the center of the condyle from the bottom of the hypertrophic zone to the top of the fibrous zone (Figure 8A-D). The groups were divided into experimental right, experimental left, control right, and control left, and the MCC width averages were taken for each group. The averages for each group were not statistically significant (Figure 9, and Table 6). The experimental right condyle, which was the side of extractions, averaged 163.4 μm, while the control right condyle averaged 152.04 μm. The experimental left condyle averaged 151.58 μm, versus the control left condyle that averaged 161.7 μm. There are also no changes in appearance or density of the chondrocytes and no changes in width of the different cell layers between the four groups.

Bulk RNA-Sequencing of the MCC from mice with maxillary right molar extractions and control at 3 weeks show differential expression of genes due to extraction

We wanted to explore which genes were upregulated or downregulated right after extractions to examine if there were any molecular changes to the MCC that would indicate condylar adaptation. The bulk RNA sequencing experiment utilized a different set of mice, in

which the extractions were performed at 3 weeks of age and the mice were collected two days later. The 3-week extraction timepoint was utilized for the bulk RNA Seq experiment since the Goodwin Lab reported significant changes in the MCC cellular organization at this timepoint (Chen, 2022). RNA-sequencing was performed and 118 genes were found to be significantly, differentially expressed with a false discovery rate <0.05. This list of differentially expressed genes was further narrowed to 23 genes with at least 1 N>100 counts and $1.5 < \log2FC < -1.0$, which suggested biologically significant expression and fold change. All of these 23 genes were significantly downregulated in the extraction group compared to control, and there were no significantly upregulated genes. The 23 genes can be found on Table 5. Many of these genes have not been reported to be expressed in the TMJ/MCC, and so preliminary RNAscope experiments were performed in control samples to visualize where the genes are expressed within the TMJ and MCC. Of the 23 genes, *Scara5*, *Iqgap2*, and *Cxcl14* probes were used to test the sensitivity of the probes and develop a protocol as well as visualize the expression pattern. *Scara5* was found throughout the proliferative layer of the MCC (Figure 10), while *Cxcl14* was only found in the superficial layer (Figure 12). Even though *Iqgap2* plays a role in cell-to-cell adhesion, cell proliferation, migration, and regulation of the cytoskeleton, it was only found within a few hypertrophic chondrocytes (Figure 11). The cell-specific expression pattern of these genes in the MCC is noteworthy and warrants further RNA scope experiments in both control and extraction samples.

DISCUSSION

We utilized the mouse extraction model to induce a mandibular functional shift and to assess for condylar changes in response to this altered occlusion. A previous study by Chen et al. (2022) first established the mouse extraction model to induce a mandibular functional shift. In their study, the mice had extractions of the maxillary right molars done at 3 weeks of age, which is the age when molars have just erupted. The mice were analyzed at 6 weeks of age when mice are still not considered skeletally mature yet. These mice underwent considerable growth between 3 to 6 weeks of age, and it was found that extractions of the maxillary right molars resulted in changes in shape of both condyles, and cellular changes at the MCC bilaterally, with a shift towards mature chondrocytes. These data suggest the unilateral maxillary extraction in growing mice affected both growth and adaptation of the condyles. The goal of the current study was to assess the effect of molar tooth extraction on adaptation of the condyles in mature/adult mice with stable occlusion, without the effects of growth. In the current study, maxillary right molars were extracted at 8 weeks old when the mice are considered skeletally mature, and analysis was done 3 weeks post extraction at 11 weeks. In the adult mice with extractions, no shape changes were noted in the skull or either condyle, and no cellular changes were found in the MCC. These data indicate that no adaptive changes to the condyle ensue if an altered occlusion induced by extractions occurs when the occlusion is stable at skeletal maturation.

This result was not what we had hypothesized, and there are several possible explanations. One consideration is that three weeks was not long enough to see any physical or cellular changes due to an altered occlusion from tooth extractions. After skeletal maturation, it might take longer for the body to respond or adapt to changes, compared to a rapidly growing mouse. Future studies need to be conducted in which extractions are performed on mice at 8 weeks of age and then examined six to twelve weeks later to assess for condylar adaptation. Another possibility is that once the occlusion is stable, unilateral maxillary molar extraction is not

15

enough of an insult to affect the condylar homeostasis. A greater insult such as unilateral

maxillary and mandibular molar extraction or bilateral maxillary extraction may affect the

condyles. Overall, these data suggest occlusion is stable at 8 weeks, and malocclusion induced

by unilateral maxillary molar extraction in this context does not disrupt TMJ homeostasis.

In order to further understand the molecular changes associated with the condylar shape

and MCC cellular changes with unilateral maxillary molar extraction in growing mice, bulk RNA-

sequencing was done on the MCC from extraction and control mice 2 days following extraction

at 3 weeks of age to investigate immediate gene regulation changes. Bulk RNA sequencing of

an altered occlusion mouse MCC had not been previously done. The RNA-Seq experiment

generated a list of 23 genes (FDR<0.05, at least 1 N>100 counts, and 1.5 < log2FC <–1.0), and

all of these genes were significantly downregulated in the MCC from extraction samples

compared to control. Many of the significantly downregulated genes that were found have not

been reported to be expressed in the mouse MCC or TMJ before, and thus, provide interesting,

potentially novel, genes and signaling pathways involved in MCC adaptation/growth. Here, I

discuss the genes differentially expressed in the MCC with tooth extraction, identified by the

RNA-seq experiment, and preliminary experiments to determine the expression of these genes

in the TMJ/MCC utilizing RNA Scope.

Of the 23 differentially expressed genes, to date, we have tested RNA expression of 3,

Scara5, *Iqgap2*, and *Cxcl14*, on control (non-extraction) sections of the TMJ in 3-week old mice,

using RNA Scope with mouse specific probes against these genes. The *SCARA5* gene, also

known as Scavenger Receptor Class A Member 5, encodes proteins for scavenger receptors

(Alquraini, 2020). Scavenger receptors are cell-surface proteins that bind to a wide range of self

and non-self ligands to affect many processes including innate immunity, maintaining cellular

homeostasis, and lipid metabolism. *SCARA5* is expressed in many organs and tissues, but

higher levels are found in fat, colon, and bladder. More recently, *SCARA5* has been studied to

gain a deeper understanding of their role in disease processes, including degenerative and

16

autoimmune diseases, and as a tumor suppressor. *SCARA5* has been shown to clear away cell debris, foreign particles, pathogens, and pro-inflammatory molecules (de Seny, 2021). De Seny et al. found the expression of *SCARA5* within healthy synovial membranes and possibly decreased levels in rheumatoid arthritis (RA) biopsies. These data may suggest that low levels of *SCARA5* are associated with inflammatory diseases since one of their functions is to remove pro-inflammatory markers. In our study, *Scara5* was expressed specifically within the proliferating chondrocytes of the control mice. The specificity of the expression suggests a specific, yet unknown, role within these cells. Since *Scara5* encodes for scavenger receptors, they could potentially assist in mediating chondrocyte proliferation and differentiation, or are merely present to remove cellular debris. More research is warranted to further our understanding of the expression of *SCARA5* in chondrocytes of articular cartilages in both healthy and diseased TMJs. It will be particularly interesting to study its expression pattern in animal models with altered occlusion.

The *IQGAP* genes encode a family of scaffold proteins that bind to the cytoskeleton to facilitate intracellular signaling and intracellular interactions (Hedman, 2015). *IQGAP1* is ubiquitous, but *IQGAP2* is mainly expressed in the liver, while *IQGAP3* is predominantly expressed in the brain. The roles of *IQGAP2* are still not as well known as *IQGAP1*, but the majority of evidence shows that *IQGAP2* acts as a tumor suppressor gene, and so a low expression of *IQGAP2* is associated with a worse cancer prognosis (Song, 2023). While *IQGAP2* is largely expressed in the liver, it can be found in many organs, but there is no research regarding its expression in articular joints. In our study, *Iqgap2* was sporadically expressed in a few hypertrophic chondrocytes in the control mice. It is interesting that this gene was only found around the hypertrophic chondrocytes and not around proliferating or mature chondrocytes, considering it assists with cell-to-cell adhesion, cell proliferation, and migration. Future studies are needed to examine the role of *Iqgap2* in hypertrophic chondrocytes within the articular cartilage, particularly whether they assist with signaling pathways to break down the

surrounding cartilage matrix for bone mineralization and chondrocyte apoptosis.

The *CXCL14* gene encodes proteins that help regulate immune cell migration and inflammatory processes (Lu, 2016). *CXCL14* acts as a chemokine to attract monocytes to sites of injury or inflammation to trigger an immune response for tissue repair and healing. *CXCL14* is also a known tumor suppressor gene, as it promotes apoptosis of cancer cells and inhibits the formation of new blood vessels. Lui et al. (2015) closely examined the gene expression of the articular cartilage from the proximal tibias of 1-week-old mice and found that *Cxcl14* was upregulated in the middle zone where the chondrocytes are rounded, scattered, and undergo cell proliferation. Chen et al. (2010) noted that *Cxcl14* was significantly upregulated in inflamed joints of arthritis-induced mice. They also found that the overexpression of *Cxcl14* exacerbates arthritis in these mice. Their study was not specific to a single joint, though. In our study of the MCC in 3-week-old control mice, we expected to find expression of *Cxcl14* within the proliferative layer, but it was only found in the superficial layer. The superficial layer is denser than the other layers because the chondrocytes are flat and elongated to provide structural support and to evenly distribute forces along the condylar cartilage during joint movement. The superficial layer also contains slow-cycling progenitor cells (Candela, 2014). Perhaps *Cxcl14* activity is decreased in progenitor cells, but further studies are needed to investigate *Cxcl14* expression and its role in articular chondrocytes.

As mentioned, expression in the MCC was explored in only 3 of the differentially expressed genes to date. Here, I discuss the remaining 20 differentially expressed genes. Preliminary literature review indicates a potential relationship between some of the genes and condylar adaptation, inflammation, and TMDs. The remaining genes will be discussed based on four broad categories: gene expression in bone and cartilage, expression in patients with rheumatoid arthritis (RA), expression during an immune response, and expression with cancers and syndromes.

The *SOST* gene encodes sclerostin, which is produced by osteocytes and has been

shown to inhibit the differentiation of pre-osteoblastic cells, thereby decreasing bone formation (Hinton, 2009). Sclerostin is already a protein of interest in the treatment of osteoporosis, so further research should investigate its potential to help condylar remodeling. *IGF1* encodes for one of the most important hormones that are key to animal growth and the anabolic pathway, and is vastly present in bones and cartilages, including the MCC (Liu, 2022). Liu et al. (2022) induced unilateral mastication in 4-week old rats by applying composite resin splints to the molars and found decreased expression of *Igf1*. These results are similar to our study in which we found downregulation of *Igf1* in the experimental mice. Suzuki et al (2003) found that local injection of *Igf1* into the condyle of mature rats resulted in increased thickness of the cartilaginous layer with more endochondral bone growth. Therefore, *IGF1* should be explored as a potential therapeutic target. *P2RY13* is found in many organs but can also be found in bone marrow cells as it has been implicated in bone remodeling (Dsouza, 2021). Lower expression is associated with reduced bone turnover, so *P2RY13* may also be a potential therapeutic target for osteoporosis, bone diseases, and condylar remodeling. *COL14A1* helps regulate fibrillogenesis, but there is not much information regarding its specific influence in the mandibular cartilage, so further research is needed (Alcaide-Ruggiero, 2021). Recent evidence on *GAS7* suggests it plays a role in mesenchymal chondrogenesis (Chang, 2008). Deletion of *RSPO3* gene has been found to cause cleft palates, mandibular incisors hypodontia, and hypoplastic mandibles, so further research is warranted to see how this gene may affect mandibular condylar growth and the MCC (Dasgupta, 2021).

Many of the genes we found are associated with rheumatoid arthritis, which is a common autoimmune disease that can affect the TMJ and cause TMDs. *CLEC5A* is mainly expressed by myeloid cells and has primarily been studied in its roles against viruses (Joyce-Shaikh, 2010). However, it is also known to play a critical role in the inflammatory response associated with RA, as its upregulation recruits immune cells to the joint to promote bone erosion. The *FCGR3* gene encodes for IgG activating receptors on many immune cells and high

levels are thought to induce osteoclastogenesis under inflammatory conditions, such as RA

(Zuo, 2021). A very prominent surface marker found on immune cells and tumor cells is *CD83*,

and elevated levels of soluble *CD83* were detected in the synovial fluid of RA patients (Grosche,

2020). The gene *PI16* was found to be upregulated in the synovial fluid and synovial tissue of

RA patients, compared to patients with OA or healthy controls, so it may play a role in the

inflammatory process or RA (Wang, 2024). Additionally, *Pi16* was found to be associated with

chronic pain in the spared nerve injury induced mouse model (Singhmar, 2020). Hepatocytes

are the primary producers of *LBP*, where it then circulates through the bloodstream as an acute-

phase response to an infection or inflammation (Huang 2018). *LBP* is used as a biomarker for

both OA and RA and was found to be highly expressed in the synovial fluid of RA patients, even

more than OA patients (Wen, 2018). It would be interesting to see how *LBP* expression levels

correlate with different levels of TMJ pain.

      LYVE1 is a major receptor for hyaluronic acid (HA) within lymphatic vessel walls and

plays a critical role in modulating immune cell migration (Banerji, 1999). Further investigation is

needed to see if *LYVE1* binds to HA within the condylar cartilage. One of the first

subcomponents of the complement pathway is *C1Q*, which is composed of three polypeptide

chains: *C1QA*, *C1QB*, and *C1QC*. Our study found significant downregulation of *C1qa* and

C1qc. Lubbers et al. (2020) found that murine primary chondrocytes can express all the genes

required to make *C1q*, but *C1qc* is highly expressed in OA-induced mouse articular

chondrocytes. However, *C1QC* and *C1QA* have not been studied in RA or other inflammatory

disease models, so there is potential for further research with these genes.

      Many genes act as tumor suppressors, so dysregulation or downregulation may be

associated with malignancies. *CCDC3* is a protein mainly secreted by vascular endothelial cells

and adipose tissues and functions as a tumor suppressor and aids in anti-inflammation (Omari,

2023). Reduced levels of *GLIPR2* have been strongly associated with a spectrum of

malignancies (Lin, 2024). Overexpression of the *KCNAB2* gene, which affects voltage-gated

potassium channels, has been found to be involved in numerous cancers and is being investigated as a therapeutic target (Lyu, 2022). *CD248* is mainly expressed on pericytes and fibroblasts during development and is mostly absent in normal adults, while overexpression is seen in cancer tissues (Teicher, 2019). The remaining two genes are strongly associated with syndromes, so even though initial research does not show a relationship between these genes and TMDs, future studies are needed to further investigate their potential roles. A mutation in the *FBN1* gene is associated with Marfan syndrome, which is a connective tissue disorder that mainly affects the musculoskeletal, cardiovascular, and ocular systems. *GATM* is involved in creatine biosynthesis, but a mutation of this gene results in creatine deficiency syndrome, which affects the entire nervous system (Baker, 2021).

The goal for future studies is to develop RNAscope protocols with probes against the remaining differentially expressed genes of interest. The highly specific expression of the genes explored so far suggest important, yet unknown, roles for these genes in specific chondrocyte populations. These genes may serve as specific markers of chondrocyte populations, adding to our tools for identification and lineage tracing of these populations. As discussed, many of these differentially expressed genes play roles in inflammation, immune response, and bone and cartilage remodeling, yet their roles in the TMJ specifically are not known. It will be interesting to further study these genes in order to increase our understanding of the cellular changes and genetic pathways involved in condylar adaptation, particularly after skeletal maturation. We believe the unilateral maxillary molar extraction mouse model is useful for the study of TMJ adaptation in response to malocclusion. The tooth extraction mouse model continues to show advantages over previous animal studies which induced an altered occlusion by other means. Numerous studies utilized larger animals, including primates, sheep, rabbits and pigs, but mice are economical, readily available, easy to genetically modify, and more manageable to house and care for than larger animals. Prior animal models that studied occlusion related TMDs mainly used oral appliances to induce an altered occlusion, but oral appliances are technique

sensitive and heavily dependent on the operator. Tooth extraction models are also the most relatable to clinical scenarios, since many patients lose teeth either naturally, by accident, or for orthodontic treatment.

In terms of clinical dentistry, and more specifically, in orthodontics, this study may indicate that extractions are not the cause of post-orthodontic TMDs. Premolar extractions are common in orthodontic treatment to relieve crowding and achieve a mutually protected occlusion. Numerous studies have shown that there is no relationship between orthodontic extractions and TMDs, yet most of the population seem to believe there is still a correlation. Our study may suggest that the timing of extractions is important as our data suggest extractions in growing mice were more detrimental than in mature mice. A clinician may consider extractions in a more mature patient (teenager/adult), which is usually the case, vs a young child in a pre-pubertal growth spurt. Furthermore, although an altered occlusion, including one induced by extractions, is one of dozens of etiologies for TMDs, studies have shown that subsequent orthodontic treatment can help to relieve TMD symptoms (Shroff, 2018). Without orthodontic therapy, TMD signs and symptoms may worsen over time as the altered occlusion is not corrected to a functional occlusion.

CONCLUSION

There were no changes in morphology of the condyle and no changes to the cellular organization of the MCC in adult mice after extraction of the 3 maxillary right molars, and thus no adaptive changes occur in response to altered occlusion in skeletally mature mice with stable occlusion. The data suggests that occlusion is stable at 8 weeks, and malocclusion induced by unilateral maxillary molar extraction in this context does not disrupt TMJ homeostasis.

REFERENCES

1. Alowaimer HA, Al Shutwi SS, Alsaegh MK, et al. Comparative Efficacy of Non-Invasive Therapies in Temporomandibular Joint Dysfunction: A Systematic Review. *Cureus*. 2024;16(3):e56713. Published 2024 Mar 22. doi:10.7759/cureus.56713

2. Alquraini A, El Khoury J. Scavenger receptors. Curr Biol. 2020;30(14):R790-R795. doi:10.1016/j.cub.2020.05.051.

3. Banerji S, Ni J, Wang SX, et al. LYVE-1, a new homologue of the CD44 glycoprotein, is a lymph-specific receptor for hyaluronan. J Cell Biol. 1999;144(4):789-801. doi:10.1083/jcb.144.4.789.

4. Candela ME, Cantley L, Yasuaha R, Iwamoto M, Pacifici M, Enomoto-Iwamoto M. Distribution of slow-cycling cells in epiphyseal cartilage and requirement of β-catenin signaling for their maintenance in growth plate. J Orthop Res. 2014;32(5):661-668. doi:10.1002/jor.22583.

5. Chen CP, Zhang J, Zhang B, et al. Unilateral Loss of Maxillary Molars in Young Mice Leads to Bilateral Condylar Adaptation and Degenerative Disease. JBMR Plus. 2022;6(7):e10638. Published 2022 Jul 3. doi:10.1002/jbm4.10638.

6. Chen L, Guo L, Tian J, et al. Overexpression of CXC chemokine ligand 14 exacerbates collagen-induced arthritis. J Immunol. 2010;184(8):4455-4459. doi:10.4049/jimmunol.0900525.

7. Chisnoiu AM, Picos AM, Popa S, et al. Factors involved in the etiology of temporomandibular disorders - a literature review. Clujul Med. 2015;88(4):473-478. doi:10.15386/cjmed-485.

8. de Seny D, Baiwir D, Bianchi E, et al. New Proteins Contributing to Immune Cell Infiltration and Pannus Formation of Synovial Membrane from Arthritis Diseases. Int J Mol Sci. 2021;23(1):434. Published 2021 Dec 31. doi:10.3390/ijms23010434.

9. Dsouza C, Komarova SV. Characterization of Potency of the P2Y13 Receptor Agonists: A Meta-Analysis. Int J Mol Sci. 2021;22(7):3468. Published 2021 Mar 27. doi:10.3390/ijms22073468.

10. Hedman AC, Smith JM, Sacks DB. The biology of IQGAP proteins: beyond the cytoskeleton. EMBO Rep. 2015;16(4):427-446. doi:10.15252/embr.201439834.

11. Hinton RJ, Serrano M, So S. Differential gene expression in the perichondrium and cartilage of the neonatal mouse temporomandibular joint. Orthod Craniofac Res. 2009;12(3):168-177. doi:10.1111/j.1601-6343.2009.01450.x.

12. Huang ZY, Perry E, Huebner JL, Katz B, Li YJ, Kraus VB. Biomarkers of inflammation - LBP and TLR- predict progression of knee osteoarthritis in the DOXY clinical trial. Osteoarthritis Cartilage. 2018;26(12):1658-1665. doi:10.1016/j.joca.2018.08.005.

13. Jung J-K, Sohn W-J, Lee Y, Bae YC, Choi J-K, Kim J-Y. Morphological and cellular examinations of experimentally induced malocclusion in mice mandibular condyle. Cell Tissue Res. 2014 Feb;355(2):355-363.

14. Kirveskari P, Alanen P. Association between tooth loss and TMJ dysfunction. J Oral Rehabil. 1985 May;12(3):189-194.

15. Lai YC, Yap AU, Türp JC. Prevalence of temporomandibular disorders in patients seeking orthodontic treatment: A systematic review. J Oral Rehabil. 2020 Feb;47(2):270-280.

16. Liu Z, Hou Y, Zhang P, Lu H, Wang W, Ma W. Changes of the condylar cartilage and subchondral bone in the temporomandibular joints of rats under unilateral mastication and expression of Insulin-like Growth Factor-1. J Stomatol Oral Maxillofac Surg. 2022;123(4):405-416. doi:10.1016/j.jormas.2021.09.013.

17. Lu J, Chatterjee M, Schmid H, Beck S, Gawaz M. CXCL14 as an emerging immune and inflammatory modulator. J Inflamm (Lond). 2016;13:1. Published 2016 Jan 5. doi:10.1186/s12950-015-0109-9.

18. Lui JC, Chau M, Chen W, et al. Spatial regulation of gene expression during growth of articular cartilage in juvenile mice. Pediatr Res. 2015;77(3):406-415. doi:10.1038/pr.2014.208.

19. Mérida Velasco JR, Rodríguez Vázquez JF, De la Cuadra Blanco C, Campos López R, Sánchez M, Mérida Velasco JA. Development of the mandibular condylar cartilage in human specimens of 10-15 weeks' gestation. J Anat. 2009;214(1):56-64. doi:10.1111/j.1469-7580.2008.01009.x.

20. Shroff B. Malocclusion as a Cause for Temporomandibular Disorders and Orthodontics as a Treatment. Oral Maxillofac Surg Clin North Am. 2018;30(3):299-302. doi:10.1016/j.coms.2018.04.006.

21. Shen G, Darendeliler MA. The adaptive remodeling of condylar cartilage---a transition from chondrogenesis to osteogenesis. J Dent Res. 2005;84(8):691-699. doi:10.1177/154405910508400802.

22. Singh M, Detamore MS. Biomechanical properties of the mandibular condylar cartilage and their relevance to the TMJ disc. J Biomech. 2009;42(4):405-417. doi:10.1016/j.jbiomech.2008.12.012.

23. Song F, Dai Q, Grimm MO, Steinbach D. The Antithetic Roles of IQGAP2 and IQGAP3 in Cancers. Cancers (Basel). 2023;15(4):1115. Published 2023 Feb 9. doi:10.3390/cancers15041115.

24. Suzuki S, Itoh K, Ohyama K. Local administration of IGF-I stimulates the growth of mandibular condyle in mature rats. J Orthod. 2004;31(2):138-143. doi:10.1179/146531204225020436.

25. Teicher BA. CD248: A therapeutic target in cancer and fibrotic diseases. Oncotarget. 2019;10(9):993-1009. Published 2019 Jan 29. doi:10.18632/oncotarget.26590.

26. Zuo Y, Deng GM. Fc Gamma Receptors as Regulators of Bone Destruction in Inflammatory

Arthritis. Front Immunol. 2021;12:688201. Published 2021 Jun 23.

doi:10.3389/fimmu.2021.688201.
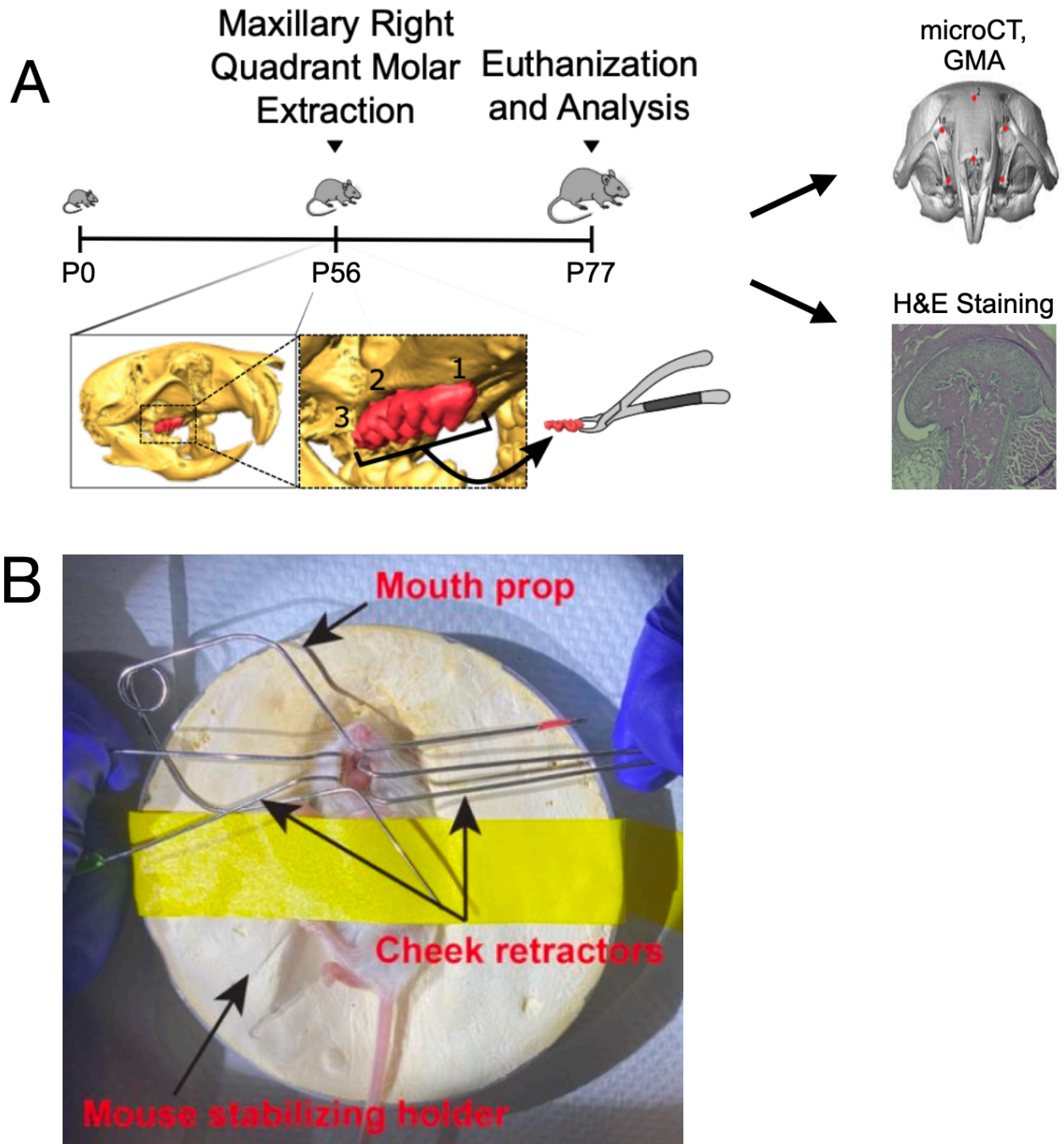
Figure 1. Experimental timeline and extraction mouse model (A) Schematic of the overall experimental design. (B) Picture of the optimized mouse tooth extraction set up as described in the Materials and Methods. (Chen et al. JBMR, 2022)
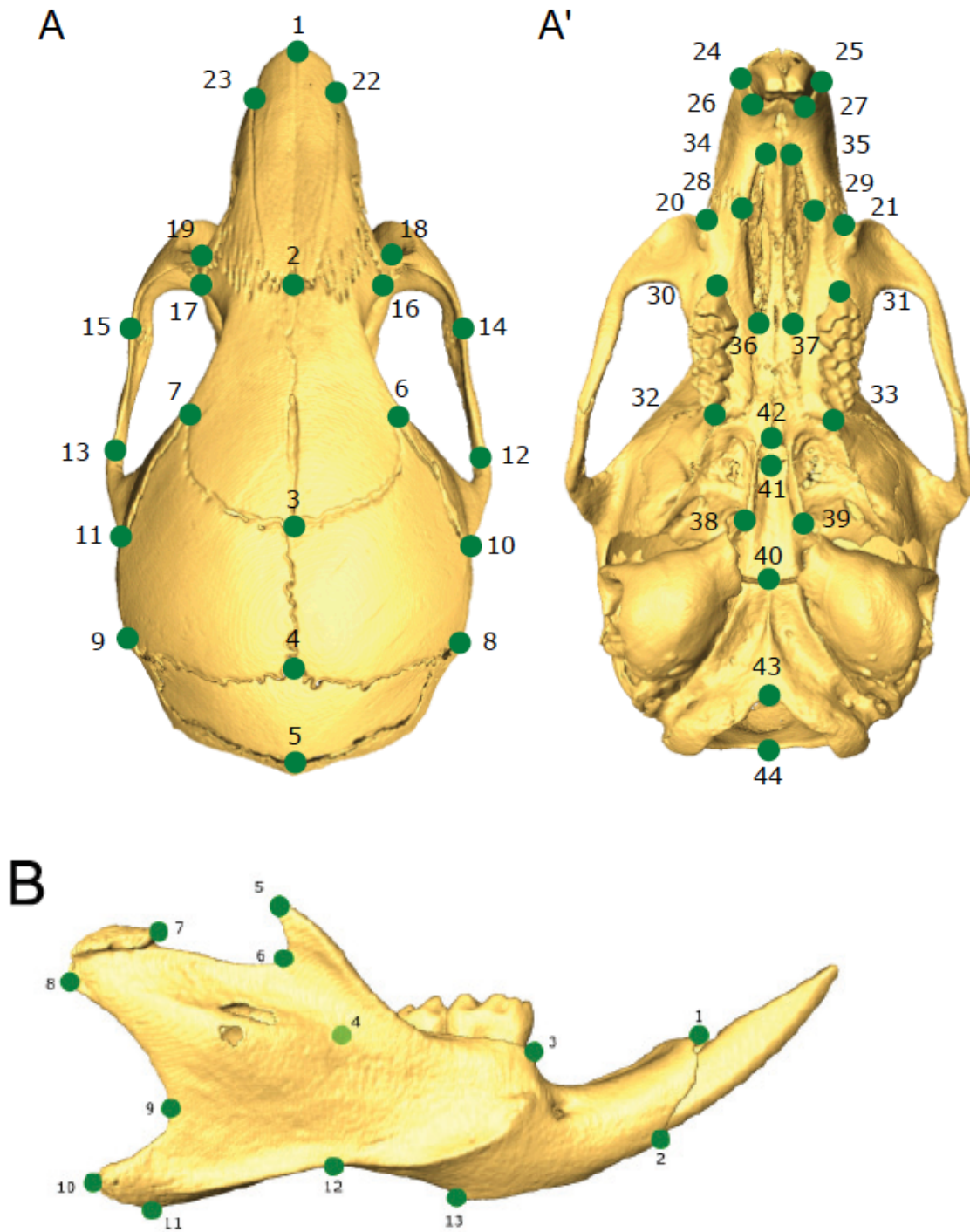
Figure 2. Landmarks used for GMA (A, A') The 44 landmarks used for the skull. (B) The 13 landmarks used for each side of the mandible. (Chen et al. JBMR, 2022)
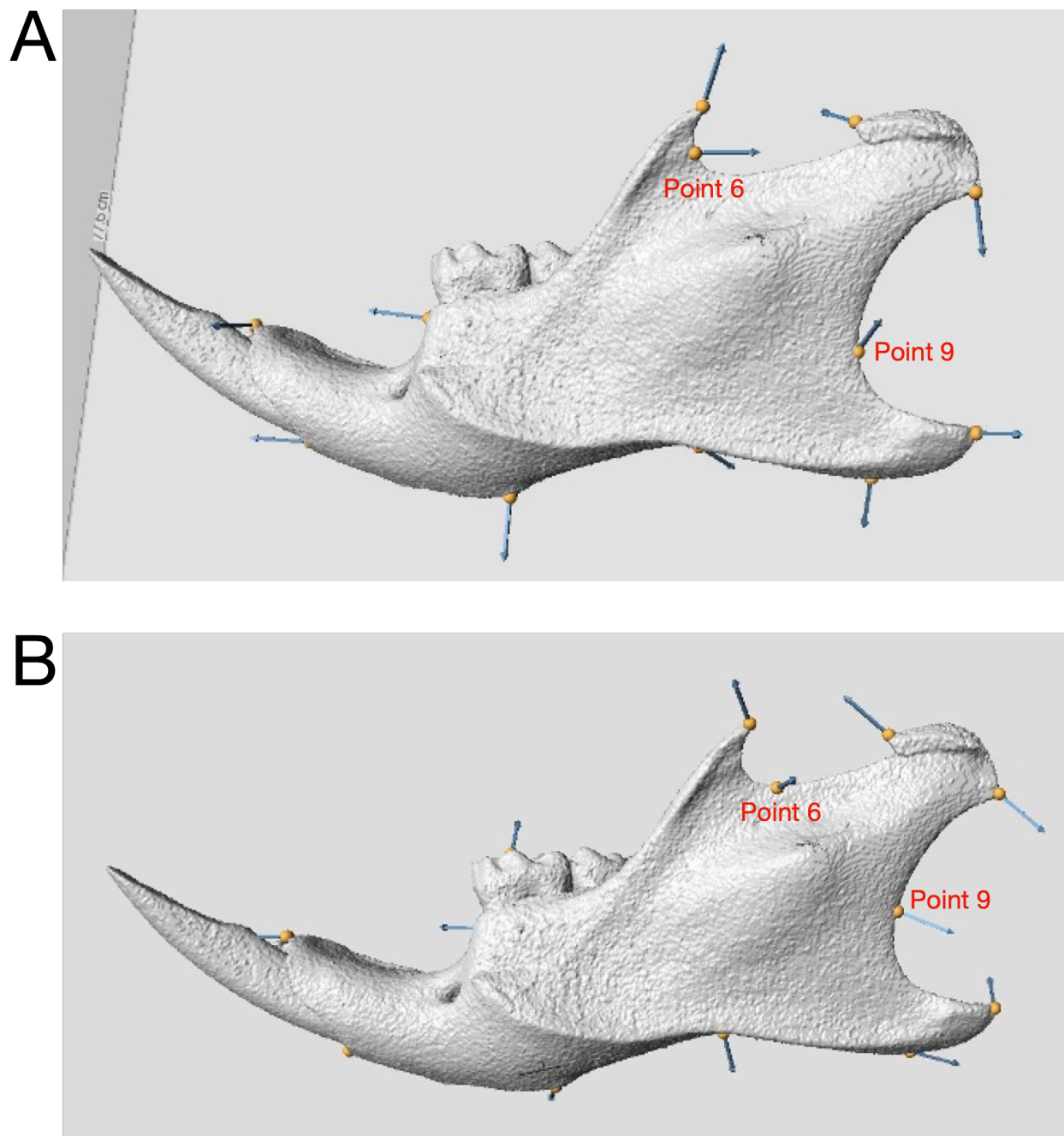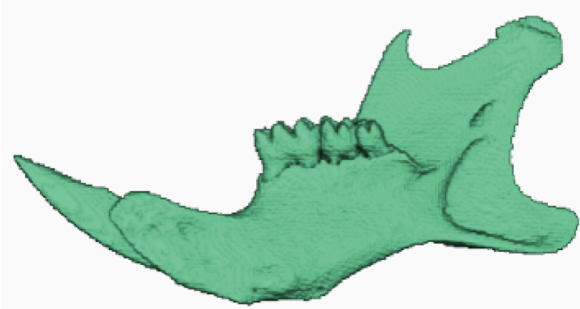
Figure 3. Inter-rater reliability tests (A) Example of left control mandible with Point 6, the most anterior/inferior concave point of the coronoid process, and Point 9, the most concave point between the condyle and angular process, as landmarked by Examiner 1 (B) The same left control mandible with Point 6 and Point 9 as landmarked by Examiner 2.

Experimental Right

Control Right
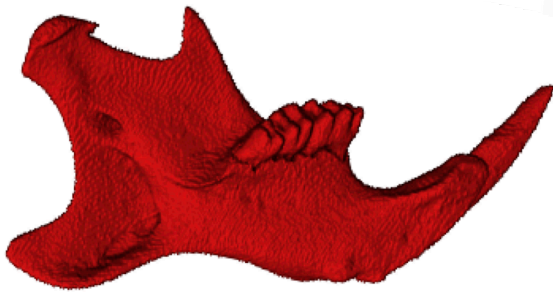
Experimental Left

Control Left

Figure 4. Representative isosurfaces (A) Comparison of the right mandible from an experimental and control mouse. (B) Comparison of the left mandible from an experimental and control mouse. Notice the similar shape of the condylar head in the left, right, experimental, and control mandibles. No morphological shape differences were found between them.
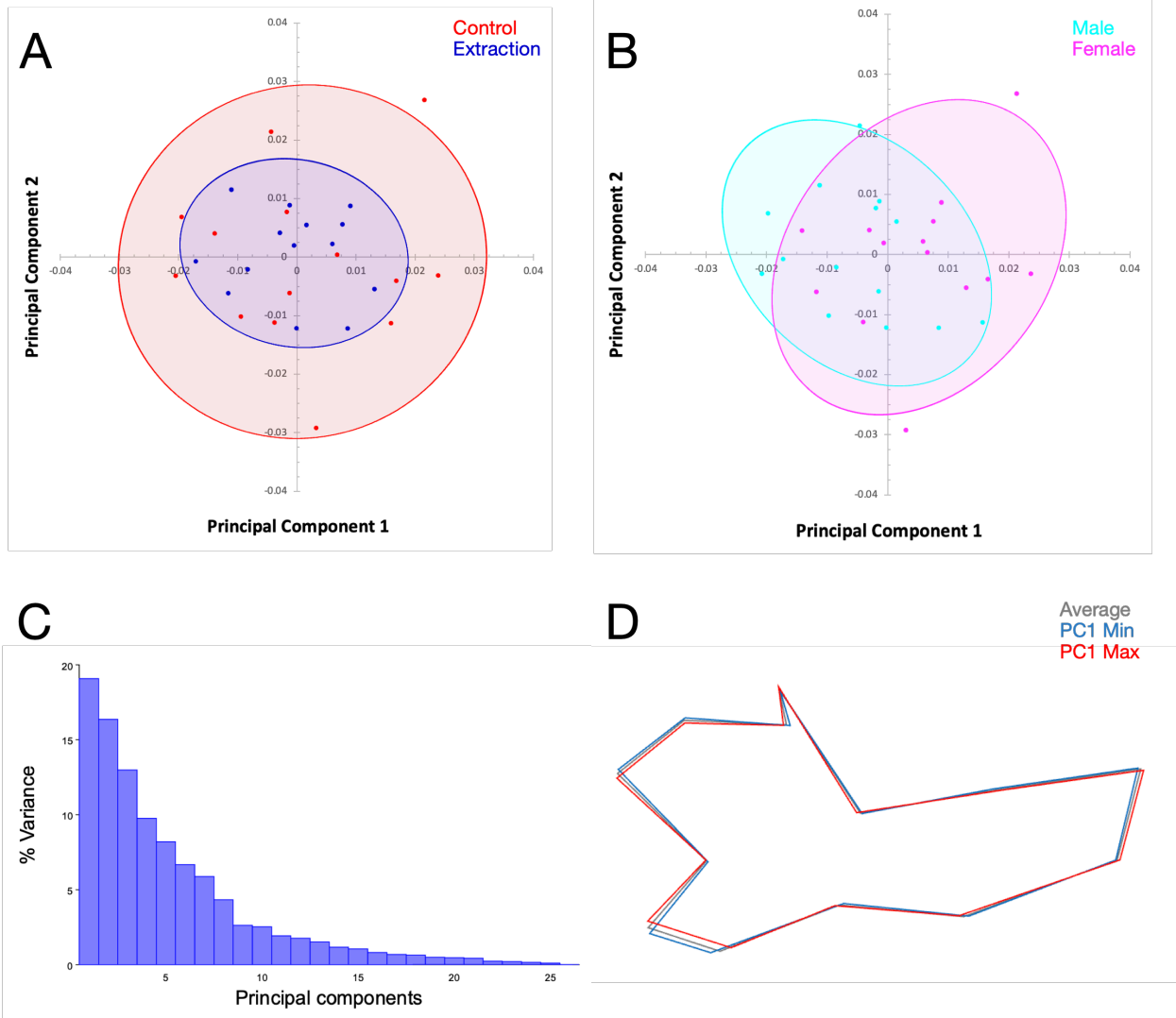
Figure 5. PCA of the left mandible (A) PCA comparing the left mandible in control (in blue) and extraction (in red) samples along PC1 and PC2. No significant differences were found. (B) PCA 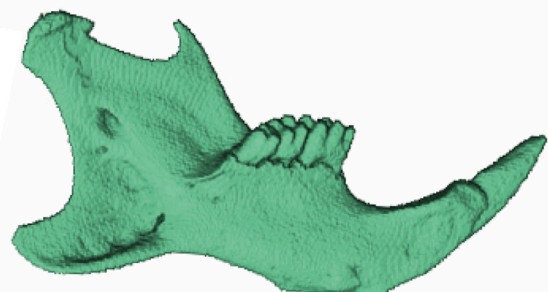comparing males (in light blue) and females (in pink), along PC1 and PC2 in regards to the left mandible. No differences were found. (C) Bar graph of all the principal component variances for the left mandible. (D) Wireframes showing the average (in gray), PC1 Min (in blue), and PC1 Max (in red) of the left mandible. No shape changes are observed.
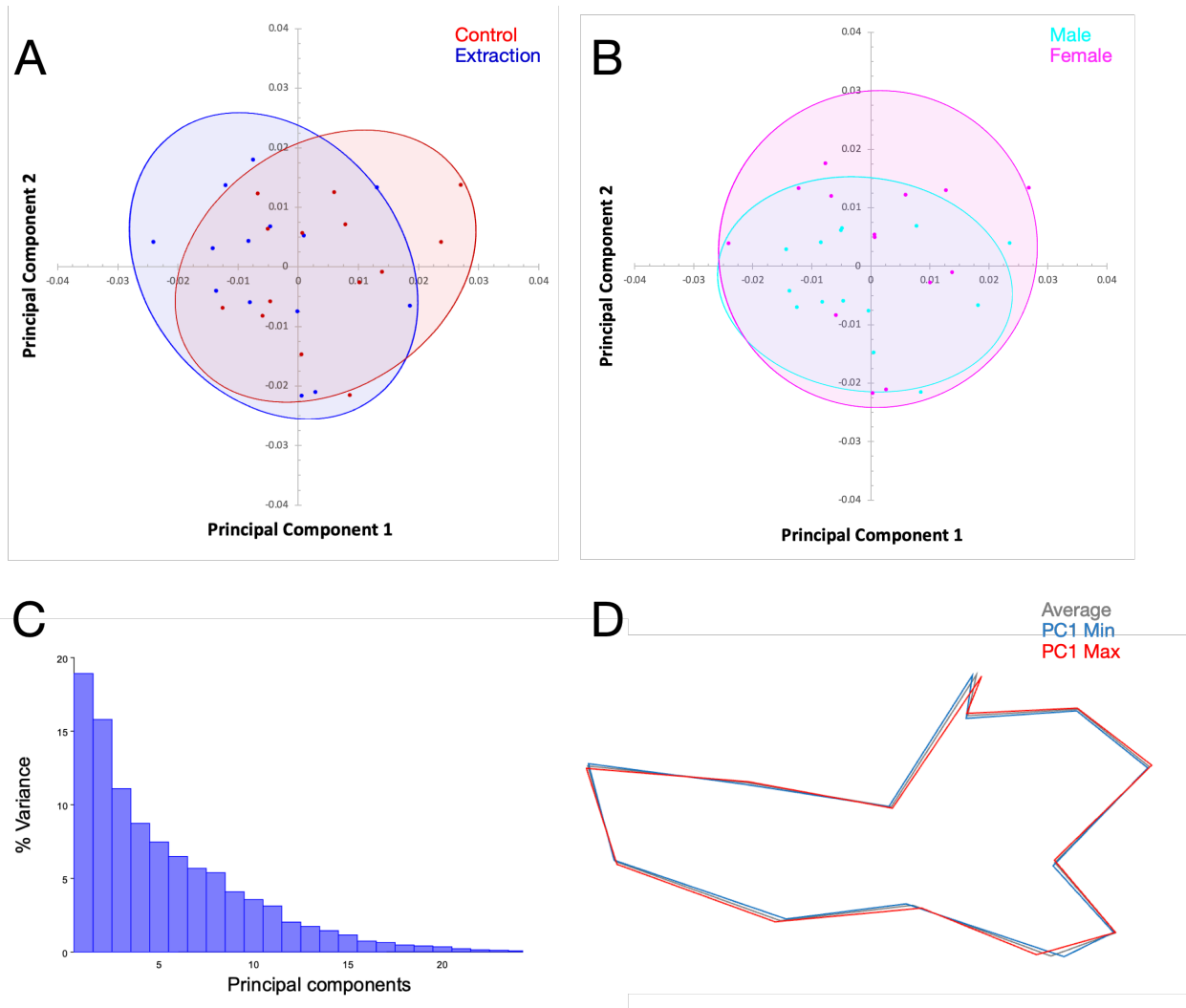
Figure 6. PCA of the right mandible (A) PCA comparing the right mandible in control (in blue) and extraction (in red) samples along PC1 and PC2. No significant differences were found. (B) PCA comparing males (in light blue) and females (in pink), along PC1 and PC2 in regards to the right mandible. No differences were found. (C) Bar graph of all the principal component variances for the right mandible. (D) Wireframes showing the average (in gray), PC1 Min (in blue), and PC1 Max (in red) of the right mandible. No shape changes are observed.
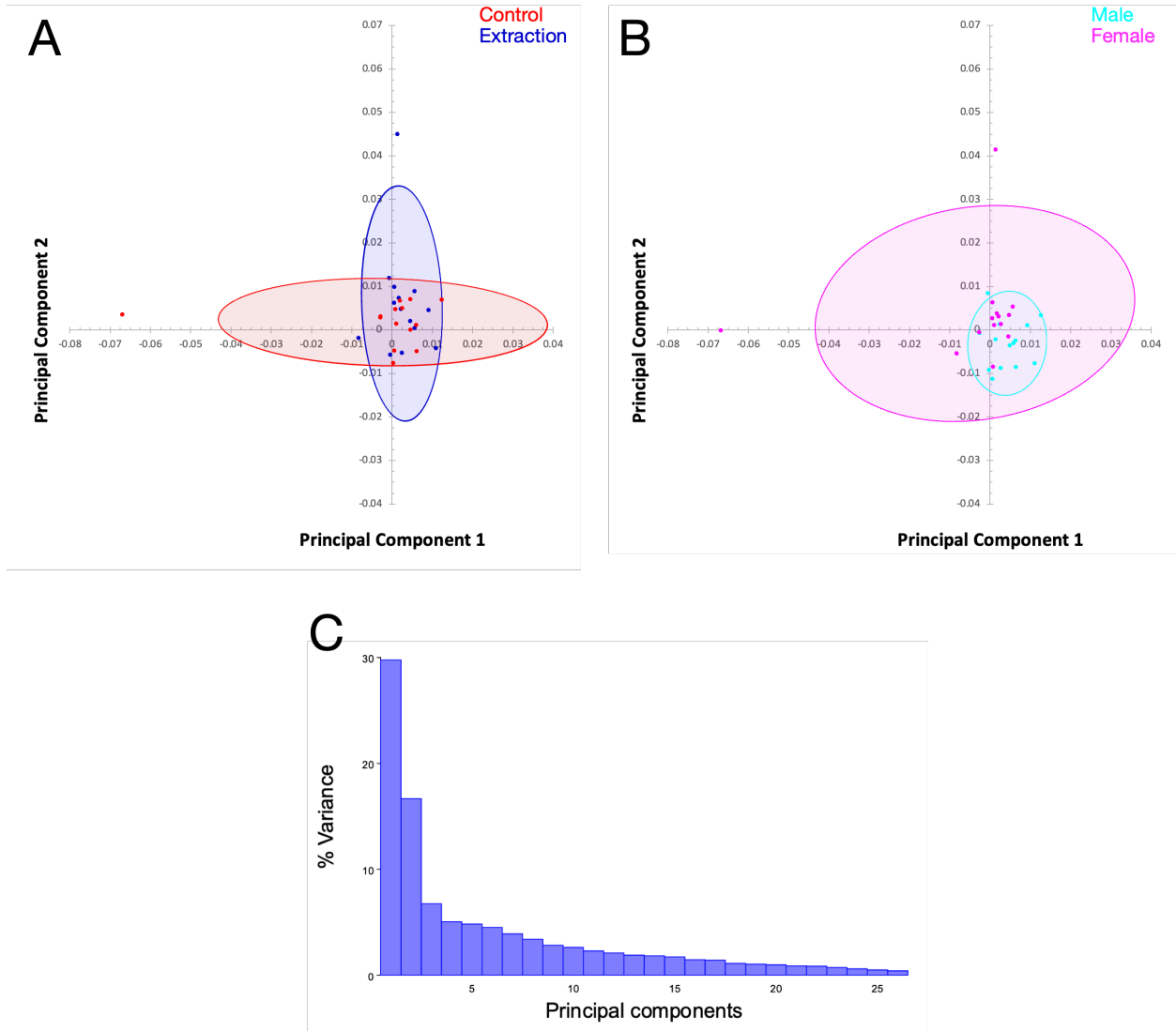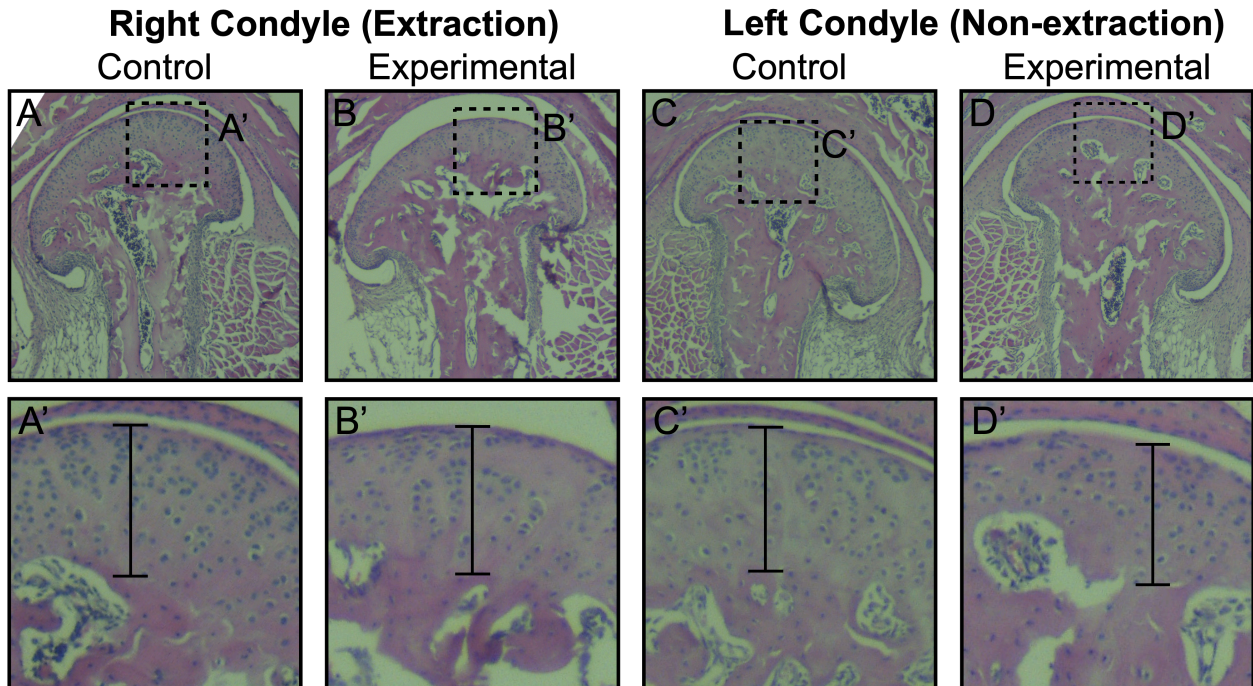
Figure 7. PCA of the skull (A) PCA comparing the skull in control (in blue) and extraction (in red) samples along PC1 and PC2. No significant differences were found. (B) PCA comparing males (in light blue) and females (in pink), along PC1 and PC2 in regards to the skull. No differences were found. (C) Gar graph of all the principal component variances for the skull.

Figure 8. Hematoxylin and eosin (H&E) staining (A-A') H&E staining of sections of the right condyle from control mice compared to (B-B') the experimental mice with extractions at 8 weeks and anesthetized at 11 weeks. (C-C') H&E staining of sections of the left condyle from control mice compared to (D-D') the experimental mice with extractions at 8 weeks and anesthetized at 11 weeks. No differences in width of the MCC or cellular composition of the chondrocytes are observed in all samples.

A
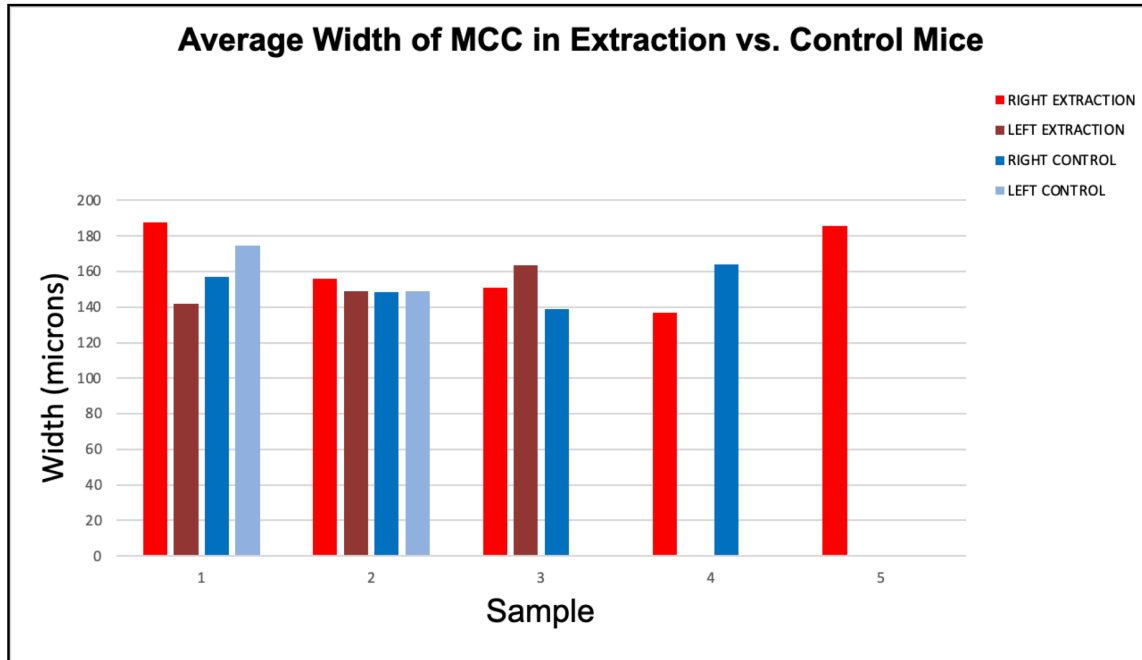
B
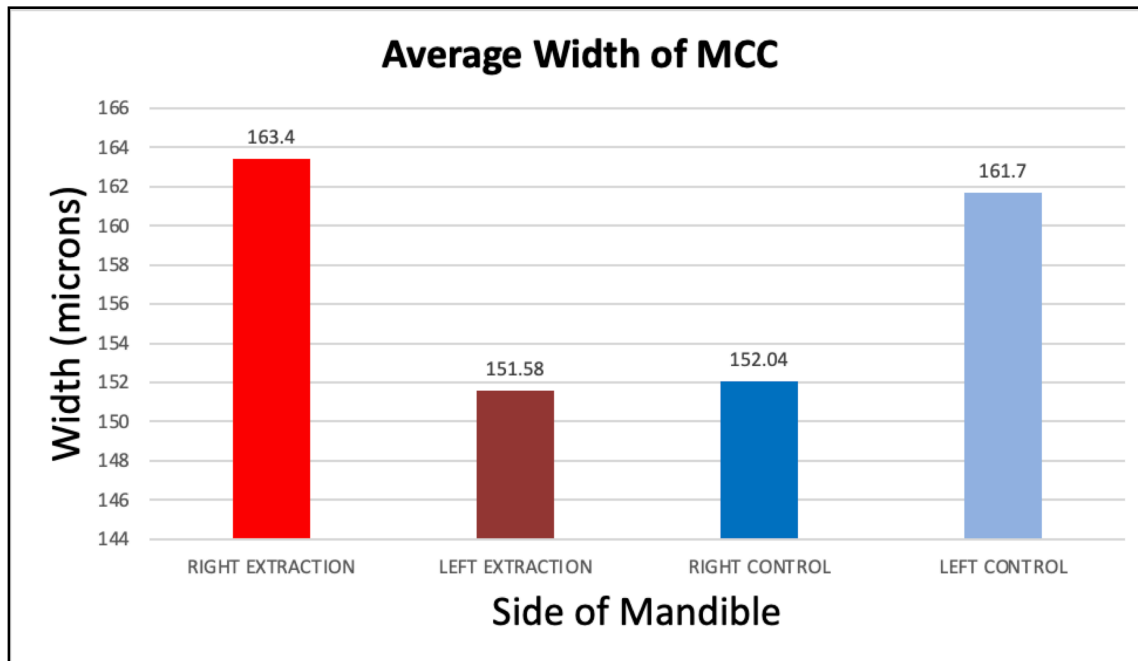
Figure 9. Bar graphs for H&E staining (A) Bar graph of the widths measured for each sample. (B) Bar graph of the average width for each side of the mandible in control and extraction mice. There is no discerning pattern observed.
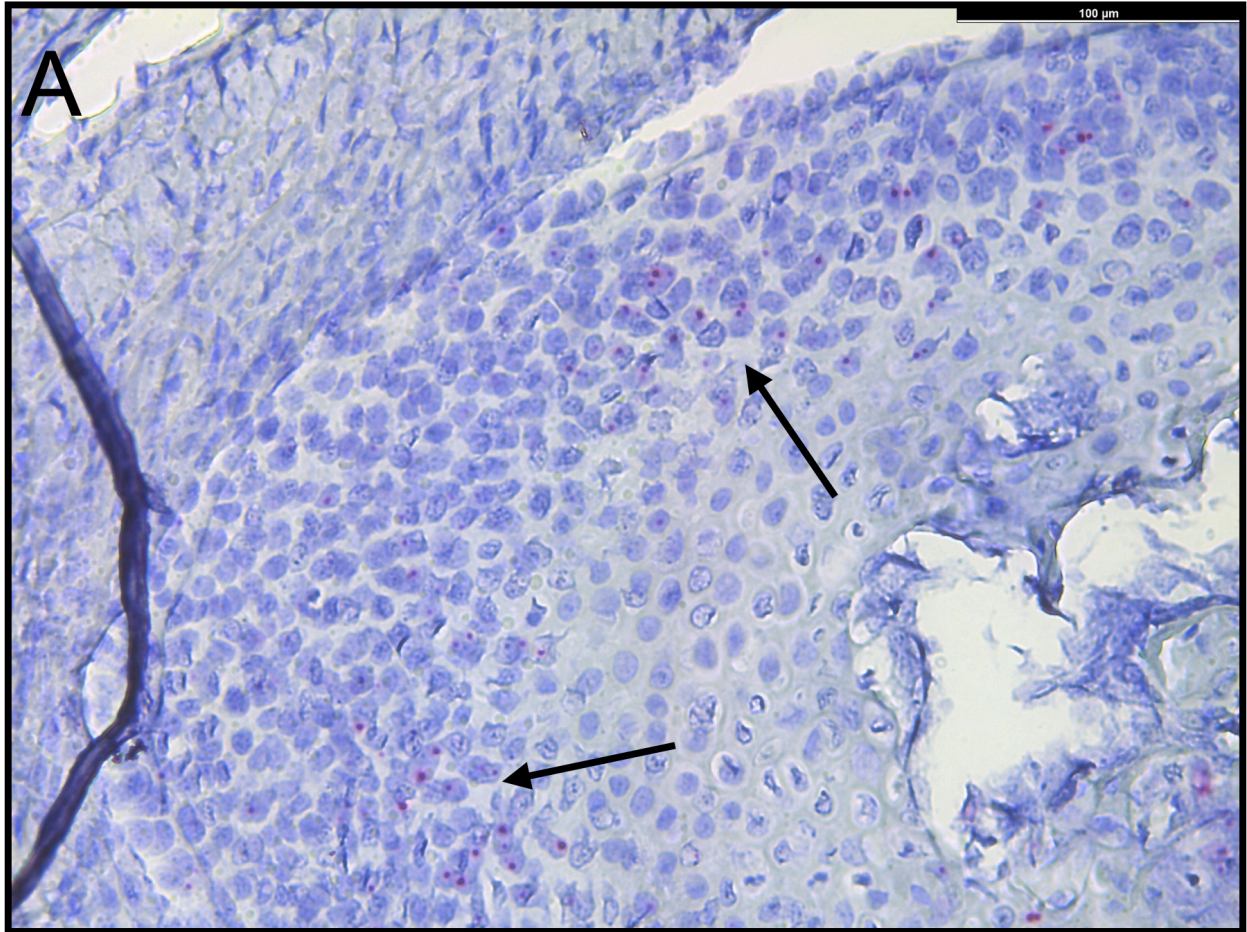
Scara5

Figure 10. RNAscope with *Scara5* on control samples of 3-week old mice. The RNAscope shows the expression of *Scara5* within the proliferative layer (pink dots).
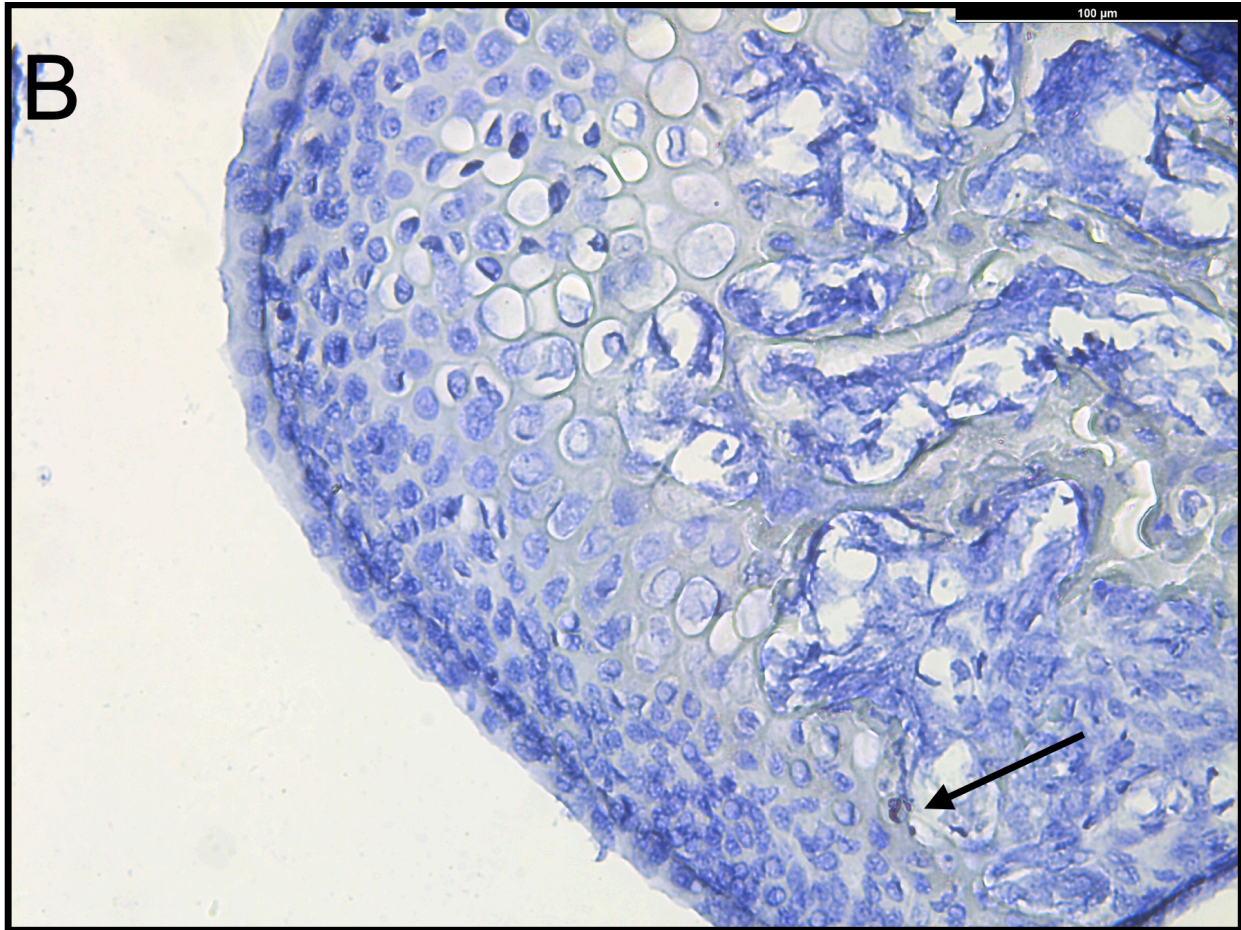
Iqgap2

Figure 11. RNAscope with *Iqgap2* on control samples of 3-week old mice. The RNAscope shows small expression of *Iqgap2* in only a few hypertrophic chondrocytes (pink dots) within the hypertrophic layer.
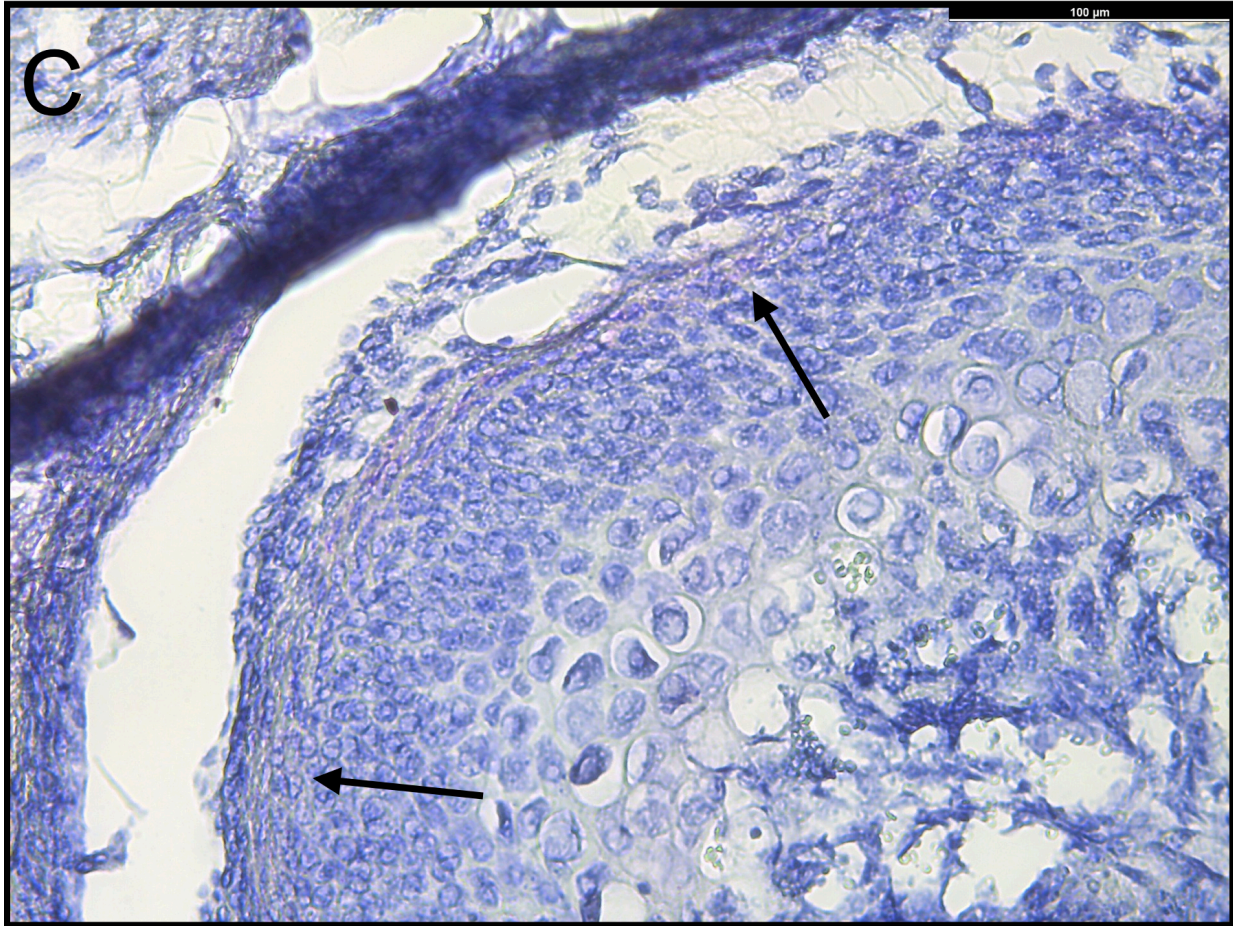
Cxcl14

Figure 12. RNAscope with *Cxcl14* on control samples of 3-week old mice. The RNAscope shows the expression of *Cxcl14* along the superficial layer only (pink dots).

TABLES

Table 1. Description of landmarks used for GMA (A) A list and description of the 44 landmarks used for the mouse skull. (B) A list and description of the 13 landmarks used for each side of the mandible. (Chen et al. JBMR, 2022)

A

Point #	Description of Landmark
1	nasal bone's most anterior suture (at midline) - most posterior intersection
2	nasal bone's most posterior suture (at midline)
3	frontal bone's most posterior suture (at midline)
4	parietal bone's most posterior suture (at midline)
5	interparietal bone's most posterior point on the median line
6	right side, most anterior point of the suture between frontal and parietal bones
7	left side, most anterior point of the suture between frontal and parietal bones
8	right side, intersection between parietal, occipital, and squamosal bones
9	left side, intersection between parietal, occipital and squamosal bones
10	right side, most posterior junction of squamosal bone & the zygomatic process of the squamosal bone
11	left side, most posterior junction of squamosal bone & the zygomatic process of the squamosal bone
12	right side, most anterior suture of jugal bone and the zygomatic process of the maxillary bone
13	left side, most anterior suture of jugal bone and the zygomatic process of the maxillary bone
14	right side, intersection of the frontal, lacrimal, and zygomatic process of the maxillary bone
15	left side, intersection of the frontal, lacrimal and zygomatic process of the maxillary bone
16	right infraorbital foramen most superior part
17	left infraorbital foramen most superior part
18	right premaxilla-nasal bone, most anterior point of suture, most superior point of nasal foramen
19	left premaxilla- left nasal bone most anterior point of suture
20	right side, intersection of maxillo-premaxillary, premaxillo-frontal & maxillo-frontal sutures, most lateral point
21	left side, intersection of maxillo-premaxillary, premaxillo-frontal & maxillo-frontal sutures, most lateral point
22	right side, most anterior point at intersection of premaxillae and nasal bones - make equal
23	left side, most anterior point at intersection of premaxillae and nasal bones
24	most superior point of the right incisor alveolus
25	most superior point of the left incisor alveolus
26	most inferior anterior point of the right incisor alveolus (middle)
27	most inferior anterior point of the left incisor alveolus (end of zig zag)
28	right premaxilla-maxilla most ventral junction
29	left premaxilla-maxilla most ventral junction
30	most anterior point of the right first molar alveolus
31	most anterior point of the left first molar alveolus
32	most posterior point of the right third molar alveolus
33	most posterior point of the left third molar alveolus
34	most anterior point of the right anterior palatine foramen
35	most anterior point of the left anterior palatine foramen
36	most posterior point of the right anterior palatine foramen
37	most posterior point of the left anterior palatine foramen
38	most inferior aspect of posterior tip of medial pterygoid process, right side
39	most inferior aspect of posterior tip of medial pterygoid process, left side
40	midline point of the suture between occipital and basisphenoid bones
41	midline point of the suture between basisphenoid and presphenoid bones
42	midline point of the suture between the palatine bones
43	foramen magnum most anterior point, basion
44	foramen magnum most posterior point

B

Point #	Description of Landmark
1	nasal bone's most anterior suture (at midline) - most posterior intersection
2	nasal bone's most posterior suture (at midline)
3	frontal bone's most posterior suture (at midline)
4	parietal bone's most posterior suture (at midline)
5	interparietal bone's most posterior point on the median line
6	right side, most anterior point of the suture between frontal and parietal bones
7	left side, most anterior point of the suture between frontal and parietal bones
8	right side, intersection between parietal, occipital, and squamosal bones
9	left side, intersection between parietal, occipital and squamosal bones
10	right side, most posterior junction of squamosal bone and the zygomatic process of the squamosal bone
11	left side, most posterior junction of squamosal bone and the zygomatic process of the squamosal bone
12	right side, most anterior suture of jugal bone and the zygomatic process of the maxillary bone
13	left side, most anterior suture of jugal bone and the zygomatic process of the maxillary bone

Table 2. PCA data of the left mandible. The PCA data includes eigenvalues and variance for each principal component. Larger eigenvalues and variances indicate principal components that were able to capture more variability within the data that account for the most important variation in the data. This data shows no significant variance.

Left Mandible	Eigenvalues	% Variance	Cumulative %
1	0.00014219	19.086	19.086
2	0.00012192	16.365	35.452
3	0.00009668	12.977	48.429
4	0.0000727	9.759	58.188
5	0.00006106	8.196	66.384
6	0.00004974	6.677	73.061
7	0.00004375	5.873	78.934
8	0.00003221	4.324	83.257
9	0.00001953	2.621	85.879
10	0.00001878	2.521	88.4
11	0.00001435	1.926	90.325
12	0.00001311	1.759	92.084
13	0.00001131	1.518	93.603
14	0.0000087	1.167	94.77
15	0.00000783	1.051	95.821
16	0.00000601	0.807	96.628
17	0.00000506	0.679	97.307
18	0.00000471	0.632	97.939
19	0.00000368	0.494	98.433
20	0.00000341	0.458	98.891
21	0.0000032	0.43	99.321
22	0.00000166	0.222	99.543
23	0.00000148	0.199	99.742
24	0.00000115	0.154	99.896
25	0.00000073	0.097	99.993
26	0.00000005	0.007	100

Table 3. PCA data of the right mandible. The PCA data includes eigenvalues and variance for each principal component. Larger eigenvalues and variances indicates principal components that were able to capture more variability within the data that account for the most important variation in the data. This data shows no significant variance.

Right Mandible	Eigenvalues	% Variance	Cumulative %
1	0.00014301	18.925	18.925
2	0.00011941	15.802	34.727
3	0.00008392	11.105	45.831
4	0.00006604	8.74	54.571
5	0.00005646	7.472	62.042
6	0.00004905	6.49	68.533
7	0.00004292	5.68	74.213
8	0.00004069	5.385	79.598
9	0.00003094	4.094	83.692
10	0.00002696	3.567	87.259
11	0.00002362	3.126	90.385
12	0.00001533	2.028	92.413
13	0.00001313	1.738	94.15
14	0.00001094	1.448	95.598
15	0.00000875	1.158	96.756
16	0.00000559	0.739	97.496
17	0.00000476	0.631	98.126
18	0.00000357	0.473	98.599
19	0.00000311	0.412	99.011
20	0.00000269	0.356	99.367
21	0.00000173	0.229	99.596
22	0.00000114	0.15	99.746
23	0.0000009	0.119	99.865
24	0.00000064	0.085	99.95
25	0.00000022	0.029	99.979
26	0.00000016	0.021	100

Table 4. PCA data of the skull. The PCA data includes eigenvalues and variance for each principal component. Larger eigenvalues and variances indicates principal components that were able to capture more variability within the data that account for the most important variation in the data. This data shows no significant variance.

Skull	Eigenvalues	% Variance	Cumulative %
1	0.00018932	29.766	29.766
2	0.00010611	16.684	46.45
3	0.00004288	6.742	53.192
4	0.00003206	5.04	58.232
5	0.00003066	4.821	63.053
6	0.0000287	4.512	67.565
7	0.00002477	3.894	71.459
8	0.00002154	3.386	74.845
9	0.00001792	2.817	77.662
10	0.00001667	2.621	80.283
11	0.00001458	2.293	82.576
12	0.00001334	2.097	84.674
13	0.00001198	1.884	86.557
14	0.00001153	1.813	88.37
15	0.00001091	1.715	90.085
16	0.00000929	1.461	91.547
17	0.00000901	1.416	92.963
18	0.00000705	1.108	94.071
19	0.00000657	1.034	95.105
20	0.00000623	0.98	96.084
21	0.00000555	0.872	96.956
22	0.00000536	0.843	97.8
23	0.00000458	0.72	98.52
24	0.00000374	0.587	99.107
25	0.00000308	0.485	99.592
26	0.00000259	0.408	100

Table 5. Significantly downregulated genes in experimental mice 2 days after extractions at 21 days. The list shows 23 genes with at least 1 N=over 100 counts and 1.5 < log2FC <–1.0 (biologically significant expression and fold change) that showed significant downregulation between control and extraction groups. RNAscope was utilized for the first three genes. The remaining genes were grouped into four broad categories: gene expression in bone and cartilage, expression in patients with rheumatoid arthritis (RA), expression during an immune response, and expression with cancers and syndromes.

		Gene	Control_1_male	Control_2_female	Control_3_male	Control_4_female	Extract_1_male	Extract_2_female	Extract_3_female	Extract_4_male
RNA Scope										
	1	Scara5	453.1	560.2	628	599.1	122.3	38.6	146.9	114.6
	2	Cxcl14	2731.3	1471.7	1618.3	1988.9	578.5	326.2	593.8	548.6
	3	Iqgap2	432	446	554.9	186.2	52.6	5.7	8.5	21.9
Bone and Cartilage										
	4	Sost	549	463.4	138.3	158.5	42.3	69.3	127.8	45.1
	5	Igf1	7491.7	4032.3	3938.6	5736.4	2165.4	1011.7	1685.1	2024.3
	6	P2ry13	13.7	145.8	91	0	0	0	0	0
	7	Col14a1	4799	2873.8	4356.1	4626.7	1442.9	773	668.8	743
	8	Gas7	958.6	900.7	1208.8	1505.1	275.5	86.4	453.2	355.4
	9	Rspo3	118.3	25	0	39.6	0	0	0	0
Rhematoid Arthritis										
	10	Clec5a	54.8	96.8	141	81.1	0	0	0	0
	11	Fcgr3	138.2	155.5	257.8	55.3	62.9	15.9	0	14.2
	12	Cd83	73.4	60.9	132.9	141.9	1.1	26.1	26.4	16.7
	13	Pi16	313.7	313.3	1463.9	971.4	59.5	304.6	67.6	399.2
	14	Lbp	756.9	613.5	1971.5	337.3	336.1	167.1	57.1	240.8
Immune Response										
	15	Lyve1	378.4	811.5	1005.4	725.3	137.2	0	127.8	78.6
	16	C1qa	423.3	580.9	1114.2	565.9	277.8	2.3	219.8	47.6
	17	C1qc	560.2	389.4	579.9	251.6	225.2	53.4	183.8	77.3
Tumor Suppressor										
	18	Ccdc3	784.3	851.7	2276.6	591.7	272.1	395.6	210.2	194.4
	19	Glipr2	193	201.2	331.9	238.7	30.9	72.7	87.7	60.5
	20	Kcnab2	242.8	142.5	289	148.4	109.8	46.6	49.7	47.6
	21	Cd248	1589.7	1774.1	2624.5	2687.5	950.1	63.7	664.6	755.9
	22	Fbn1	5675.4	4252	7492.7	11141	1917.3	1625.5	716.3	2584.4
	23	Gatm	298.8	142.5	497.8	217.5	133.8	53.4	88.7	72.1

Table 6. Width measurements of the MCC in extraction and control mice. Measurement of the widths in microns for each section. There was a lack of adequate sections due to sectioning errors, so no statistical analysis was performed. The average width for each mandible (right extraction, left extraction, right control, left control) show no significant difference or pattern.

SAMPLE	RIGHT EXTRACTION	LEFT EXTRACTION	RIGHT CONTROL	LEFT CONTROL
1	187.69	141.97	157.03	174.46
2	155.75	149.06	148.18	148.93
3	151.15	163.72	138.93	
4	136.63		164.01	
5	185.8			
AVERAGE	163.4 um	151.58 um	152.04 um	161.7 um

Publishing Agreement

It is the policy of the University to encourage open access and broad distribution of all theses, dissertations, and manuscripts. The Graduate Division will facilitate the distribution of UCSF theses, dissertations, and manuscripts to the UCSF Library for open access and distribution. UCSF will make such theses, dissertations, and manuscripts accessible to the public and will take reasonable steps to preserve these works in perpetuity.

I hereby grant the non-exclusive, perpetual right to The Regents of the University of California to reproduce, publicly display, distribute, preserve, and publish copies of my thesis, dissertation, or manuscript in any form or media, now existing or later derived, including access online for teaching, research, and public service purposes.

DocuSigned by:

Jessica Huang

8CE7C1AFAD12496...   Author Signature

5/24/2024

Date